This is the author's version of an article that has been published. Changes were made to this version by the publisher prior to publication. The final version of record is available at https://dx.doi.org/10.1109/CPE-POWERENG50821.2021.9501176

EMI Filter Re-Design in a SMPS with Inductor in Saturation

Daniele Scirè
Dipartimento di Ingegneria
Università degli Studi di Palermo
Palermo, Italy
daniele.scire@unipa.it

Giuseppe Lullo
Dipartimento di Ingegneria
Università degli Studi di Palermo
Palermo, Italy
giuseppe.lullo@unipa.it

Gianpaolo Vitale
Institute for high performance computing and networking
National Research Council (CNR)
Palermo, Italy
gianpaolo.vitale@icar.cnr.it

***Abstract*—This paper analyzes the design issues of the input EMI (Electro-Magnetic Interference) filter's in a switching mode power supply where the power inductor is operated in saturation. Starting with a SMPS equipped with linear inductor, the input filter is firstly designed to comply with Standards. Then, a new inductor with a smaller core size is employed in the same SMPS to exploit saturation. The EMI filter is re-designed, taking into account the increase of EMI introduced by the non-linear operation of the inductor. Finally, the reduction of the inductor's size and cost is compared with the increased size and cost of the EMI filter.**

Keywords— electromagnetic interference (EMI) filter, Switched Mode Power Supply, power density, nonlinear magnetics, saturable core, inductor.

I. INTRODUCTION

The requirement of improving power density in Switched Mode Power Supplies (SMPSs) has encouraged researchers to better exploit electronic components; among these, power inductors offer considerable potential for interest since the increase of the operating current, beyond the linear limit defined by the manufacturer, allows the choice of a smaller core size [1], [2]. As a matter of fact, if the range of operation of a power inductor comprises the saturation (intended as the point where the differential inductance is reduced to half of its maximum value), it can be chosen with reduced size and weight [3]. On the other hand, the saturation exploitation highlights a few aspects that should be addressed with special attention when designing the converter.

The main consequence of using an inductor in its saturation region is that the impedance is not constant, but dramatically reduces its value for increasing current. When the inductor is supplied with a constant voltage (as in SMPSs), the shape of the inductor current changes from linear to cusp-like, with a strong increase after saturation is reached. Moreover, the dependence of inductor characteristics on its temperature is more severe [4], [5]; it has been shown that the operation near the saturation increases losses and, consequently, the inductor's temperature. It modifies the shape of the current through the inductor, further increasing its peak and potentially leading to thermal runaway [6]. As a consequence, the spectrum of the current through the inductor exhibits increased amplitude for all the harmonics starting from the fundamental at the switching frequency f_s, and affecting harmonics at higher frequency [7]. This aspect is of interest when dealing with power density optimization since it affects the EMI filter design; this paper is dedicated to this issue.

The literature proposes many papers dealing with input EMI filter optimization confirming that the SMPS must be considered as a whole [2], [8]–[12]. The design of such circuits influences about the 30% of the total converter weight [13], and the transfer function of the converter; hence it has a role both on its dynamic response and stability [2], [14]. A guideline for a differential-mode filter design has been proposed in [15]; besides, it shows that the differential-mode (DM) noise mainly affects the power density of the converter.

This paper analyzes the operation of a boost converter comparing the effects on the input filter design of two inductors with the same value, one operated in linear zone and the other in saturation.. The inductor operated in saturation has a smaller rated current and, consequently, a smaller size and cost. The input differential mode EMI filters are designed for both case studies following the approach of [15]. The design considers commercially available components, comparing the increase in size and cost with the saving given by the inductor.

The paper is organized as follows: section 2 describes the operation of a SMPS with an inductor operated in saturation, section 3 describes the case studies; section 4 is dedicated to the design of the input EMI filter, section 5 shows the measurement operated by a Line Impedance Stabilization Network (LISN). Finally, sections 6 and 7 give the results and a comparison between the two case studies is proposed in section 8.

II. SMPS WITH INDUCTOR OPERATED IN SATURATION

A SMPS operates by imposing two different voltage levels to a power inductor; consequently, it experiences a DC current with a superimposed current ripple. The DC current is exploited by the load and the ripple is filtered by an output capacitor. If the inductance is constant, corresponding to the linear operation, the current has a triangular shape. Differently, exploiting saturation, the inductance varies with the current and the latter showing a higher peak value. This difference is shown in Fig. 1 where it can be noted that the two currents exhibit the same DC value meaning that the power to the load

978-1-7281-8071-7/21/$31.00 ©2021 IEEE

is the same; however, the current corresponding to saturation exploitation has a higher maximum value and a shape with increasing derivative up to the peak. Fig. 2 shows two hysteresis curves corresponding to two inductors with different saturation value; the second inductor shows the same inductance but employs a core of reduced size. In Fig. 2a the variation of the magnetic flux around the operating point causes a proportional variation on the magnetic field. Differently, when saturation is exploited, as in Fig. 2b, the magnetic field variations are more pronounced, with the same variation of the magnetic flux. Since the magnetic field is proportional to the current, the two corresponding waveforms are different. The situation of Fig 2a corresponds to an inductor exploited in linear zone, whereas Fig 2b to an inductor running in the same operating point with a lower saturation value. The modified shape of the current influences also the spectrum of the current delivered by the power source and the power switch size [7], [16].

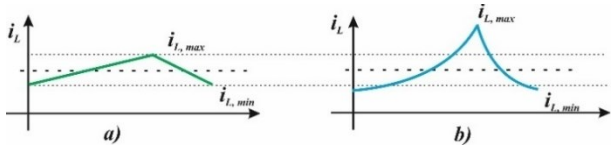

Fig. 1. Comparison of current through the power inductor: a) in linear operation, b) with saturation exploitation.

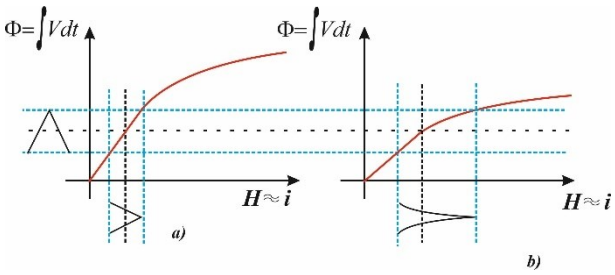

Fig. 2. Inductor operated a) in linear zone, b) near saturation: the same magnetic induction variation produces different magnetic field variations.

III. The Circuit Under Test

The power converter is a boost supplied by Vs=24 V, the switching frequency f_S is equal to 40 kHz; as power switch a MOSFET FDP12N60NZ is used, while a STTH806 rectifier is the free-wheel diode. The electric scheme is shown in Fig. 3. This converter is studied with the two inductors shown in Fig. 4. They are the models DO5040H-104 and DO5010H-104 supplied by Coilcraft [17], [18]. They have the same value of 100 µH, and are SMT Power inductors wounded on a ferrite core. The manufacturer specifies for the inductor DO5040H-104 a 10% linear threshold current (intended by the same manufacturer as the DC current at which the inductance drops 10% from its rated value) of 5.6 A. It means that the inductance can be considered as constant up to about this value. As it concerns the inductor DO5010-104, the linear threshold current is equal to 3A. However, we will extend this range adopting a 50% saturation current i.e., the current where the differential inductance is reduced to half of its maximum value, It corresponds to a maximum current of about 4 A. In this way, when operated up to 4 A, the first inductor will operate in linear zone, whereas the second will show an inductance depending on the current. Since this last approach requires a detailed characterization of the inductor that it is not delivered by the manufacturer, the inductor DO5010-104 has been previously characterized by a measurement system set up by the authors. After characterization, a suitable polynomial model for the inductor has been derived [6], [19]–[21]. The curve showing the inductance vs. current is shown in Fig. 5. The inductance of the inductor DO5040H-104 instead remains constant and it is equal to the rated inductance of the inductor DO5040H-104 for lower current, i.e., 100 µH.

The volume of the inductors can be calculated considering a cylinder with the same base of 18.54 mm for both and a height of 7.11 mm for the inductor D05010H and 12 mm for the inductor DO5040H. As a consequence, the inductor DO5010H requires approximately 1620 mm^3, whereas the inductor DO5040H requires approximately 3240 mm^3.

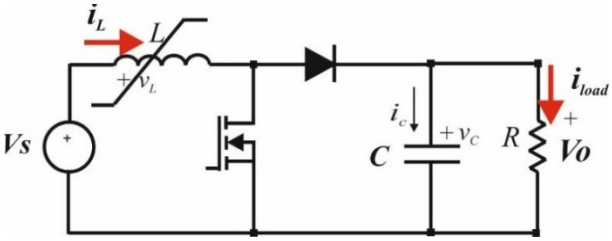

Fig. 3. Schematics of the boost converter

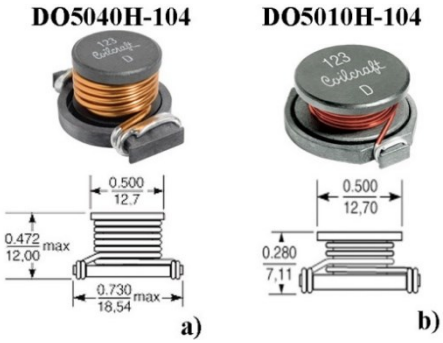

Fig. 4. The two inductors of 100 µH considered for the analysis: a) inductor with rated current of 5.6A operated in linear zone, b) inductor with rated current of 3A operated in saturation.

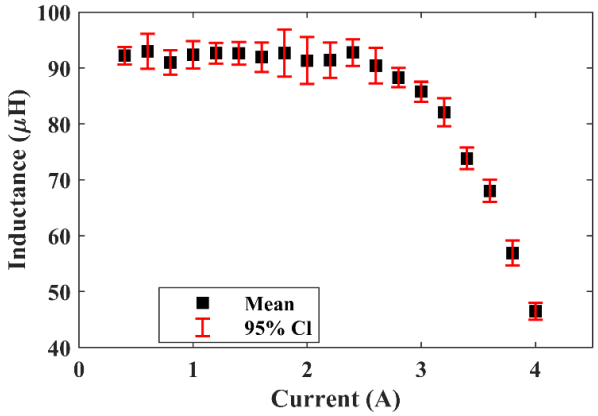

Fig. 5. Characteristic curve of the inductance versus current for the inductor DO5010H-104 obtained experimentally where the drop of the inductance can be appreciated

This is the author's version of an article that has been published. Changes were made to this version by the publisher prior to publication. The final version of record is available at https://dx.doi.org/10.1109/CPE-POWERENG50821.2021.9501176

IV. DM EMI MEASUREMENT

The differential mode EMI measurement is performed by a Line Impedance Stabilization Network. This network provides a specific impedance, standardized to 50 Ω, for measuring disturbance voltage and avoiding that the noise coming from the DC supply may influence the measure. The electric circuit scheme of the HV DC LISN is shown in Fig. 6. It is a dual DC LISN circuit configuration. The circuit is formed of two identical LISNs one for each DC power line (positive and negative wire, referred to the ground). According to CISPR 25 standard requirements [22], each LISN has an inductance, L=5 μH, a capacitor C_1=1 μF, on the mains side, and, a resistance, representing the input impedance of the measuring instrument (50 Ω), with a series connected coupling capacitor C=0.1 μF, on the DUT side [23]. The LISN has been implemented, as well as the converter under study including the non-linear model [6] of the inductor characterized in [24], [25] to verify the compliance of the filter with CISPR standard by SPICE simulation.

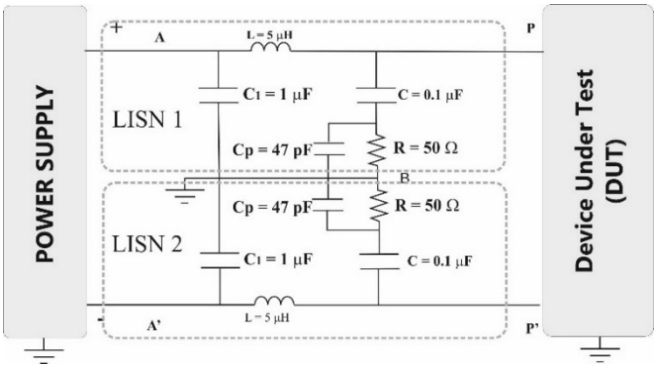

Fig. 6. Schematics of the Line Impedance Stabilization Network

V. EMI FILTER DESIGN

Conducted electromagnetic emissions are composed of DM and common-mode (CM) noise. The DM and CM generation belongs to different generation and coupling mechanism and involves different paths. In principle, separated filter sections would be required; however, it is possible to exploit the stray inductance of the CM choke for the DM filter so that they are embedded in a unique filter topology [13], [26].

The topology of an EMI filter able to lessen the CM and DM noise is shown in Fig. 7.

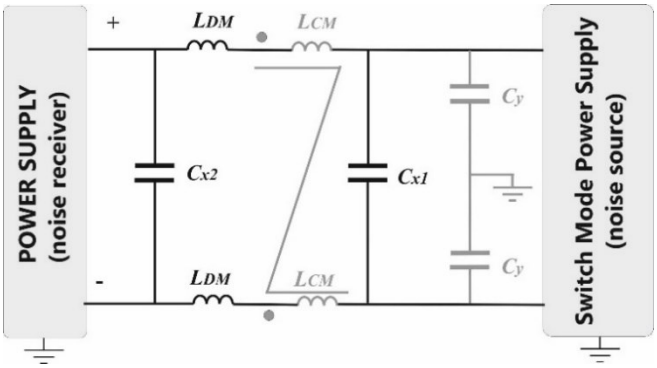

Fig. 7. Schematics of input EMI filter conceived for DM and CM noise

The capacitors C_y can attenuate both CM and DM noise; however, they are generally in the order of magnitude of nF and their effect on the DM noise is almost negligible. Differently, the capacitor C_x between the electrical lines only attenuates the DM noise. The presence of C_{x1} and C_{x2} depends on the impedance of the source and receiver [27]; in our case, only C_{x1} is used for the EMI filter; besides the analysis is achieved comparing the performance of a single and a double stage cascaded filter. The CM choke represents the bulkiest component of the filter; theoretically, its CM inductance L_{CM} acts only on the common mode, in practice its leakage inductance $L_{leakage}$ is usually sufficient to attenuate the DM noise as well [28]. Alternatively, an additional series inductance can be added.

The procedure for the CM and DM filter components design is the following. After identifying the emission peak at the lowest frequency, the attenuations for the DM and CM mode are calculated as:

$$A_{req_{att_{DM}}}[dB] = A_{h_{att_{DM}}}[dB\mu V] - Lim[dB\ \mu V] + 6dB \quad (1)$$

$$A_{req_{att_{CM}}}[dB] = A_{h_{att_{CM}}}[dB\mu V] - Lim[dB\ \mu V] + 6dB \quad (2)$$

where A_{h_att} is the amplitude of the harmonic to be attenuated, Lim is the maximum amplitude allowed by the reference standard corresponding to the frequency of interest, and an additional safety margin of 6 dB is taken into account [15]. The cut-off frequency f_o of the DM or CM filter, can be calculated as:

$$f_o = \frac{f_{h\_att}}{10^{\frac{A_{req\_att}}{filt\_att}}} \quad (3)$$

where f_{h_att} is the harmonic frequency to be attenuated and $filt\_att$ is the filter intrinsic attenuation that depends on its topology [28]. Once the corner frequency is calculated, the values of inductor and capacitor can be determined according to the following equations:

$$L_{CM} = \frac{1}{C_{CM}\left(2\pi f_{o\_CM}\right)^2}, \qquad C_{CM} = 2C_y \quad (4)$$

$$L_{DM} = (0.1 - 2)\%\ L_{CM} \quad (5)$$

$$C_{DM} = C_{x1} = C_{x2} = \frac{1}{L_{DM}\left(2\pi f_{o\_DM}\right)^2} \quad (6)$$

In this paper, only the DM filter is considered. The design procedures is based on the RMS noise current as an adequate measure for the estimation of the Quasi-Peak detection voltage at the EMI receiver [15] where, it is assumed that the total

noise current appears as a single peak only at the switching frequency and the noise voltage is calculated by multiplying it for the measuring resistance of 50 Ω. It is an approximation to simplify the filter design. In any case, the final verification of the filter performance will be carried out by means of the LISN defined by the CISPR 16 standard and shown in Fig. 6. Besides, since in the case under study, a triangular-shaped noise current is considered, the error is about equal to 0.1 dB [15]. The voltage at the LISN measurement resistance is given by:

$$U_{LISN} = 50\Omega \cdot I_{noise\_rms} \tag{7}$$

where I_{noise_rms} is the RMS of the current flowing through the power inductor of the converter minus the DC component. For a switching frequency lower than 150 kHz, the design frequency of the filter is calculated as:

$$f_D = m\, f_s \tag{8}$$

where m is a correction factor given by rounding up the ratio between 150 kHz and the switching frequency of the converter. In our case study m=4. Finally, the voltage peak at frequency f_D is calculated based on the LISN estimated voltage.

$$U_{est}(f_D)[dB\mu V] = 20\, Log\left(\frac{U_{LISN}}{m^a}\,\frac{1}{\mu V}\right) \tag{9}$$

The exponent a for triangular waveform is equal to 2 [15]. Once the U_{est} is calculated, it can be used in (1) replacing A_{h_attDM}; then the attenuation of the filter can be calculated depending on the number of cascaded stages nf so that it is greater than the required one.

$$Att_{LC}(f_D) = (2\pi \cdot f_D)^{2\cdot nf} \cdot (2L)^{nf} \cdot C_{x1}^{nf} \geq A_{req\_att}(f_D) \tag{10}$$

In this paper, since only a single and a double stage filter is considered, n is set equal to one or two.

VI. DM EMI Filtering with Linear Inductor

A. DM EMI without filter

When the inductor is operated in linear zone i.e., showing a constant inductance, its current is triangular shaped as shown in Fig. 8. The corresponding spectrum of the voltage noise evaluated on the measuring resistance of the LISN is shown in Fig. 9 with superimposed the different Class limits of the CISPR25 Standard. The RMS value of the noise current is 15.9 mA corresponding to a noise voltage on the 50Ω resistance of the LISN equal to 118 dBμV. The estimated voltage calculated by (9) with m=4 and α=2 is 93.92 dBμV; it is indicated by a dot on Fig. 9. This value is used to design the filter so that the compliance to Class 5 can be obtained. It can be noted that this value is about 30 dB higher than the corresponding spectrum line at 160 kHz.

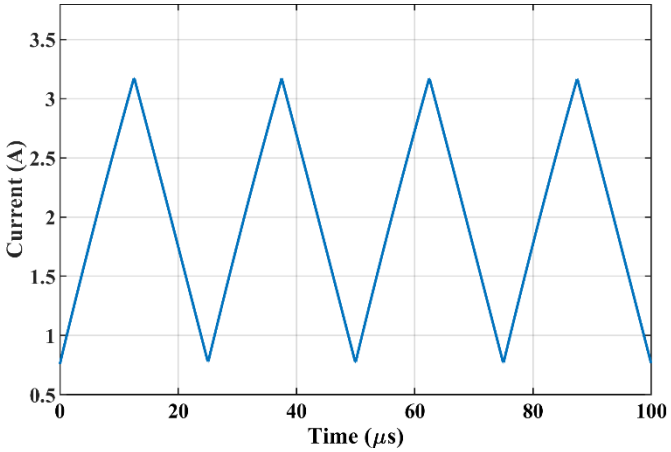

Fig. 8. Current flowing through the power inductor

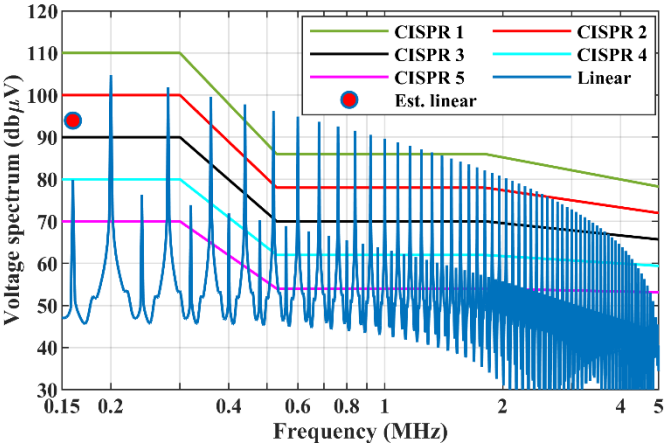

Fig. 9. Spectrum of the DM noise without filter

B. Filter design

The required attenuation calculated by (9) and (1) is 29.93 dB. The filter has been designed considering both a single and a double stage; available commercial components have been considered. All the inductors have a rated current of 3 A and the capacitor have a polyester dielectric and a rated voltage of 50 V. Both inductors and capacitors belong to the same manufacturer: RSPRO and Nichicon, respectively. The cost is referred to the purchase of a single component. The features of used components are summarized in Table I. The weight of the components was measured with a Gibertini TM8120 precision scale with an error of ± 0.02g.

TABLE I. Components of the Filter for SMPS with Inductor in Linear Operation

	Component	*Value*	*Size [mm³]*	*Cost [€]*	*Weight [g]*
Single stage	inductor	47μH	2512	0.942	9.65
	capacitor	470 nF	2194	1.091	2.51
Double stage	inductor	33μH	2267	0.895	9.49
	capacitor	100 nF	594	0.371	0.37

C. DM EMI with filter

The noise spectrum with the designed filters is shown in Fig. 10 where it can be appreciated that both filters achieve the compliance, as expected.

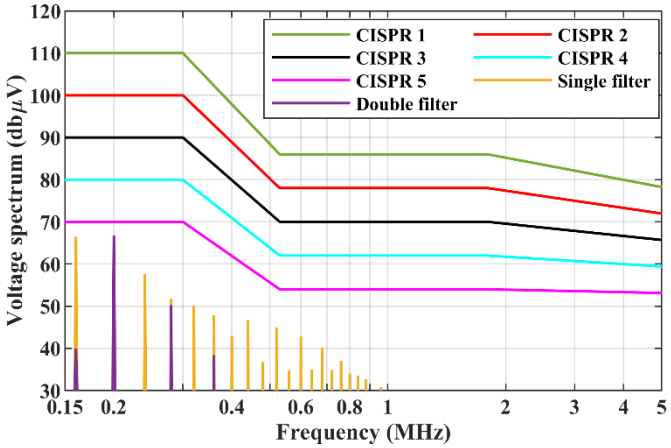

Fig. 10. Spectrum of the DM noise with filter

VII. DM EMI Filtering with Non-Linear Inductor

A. DM EMI without filter

When the inductor is operated in non-linear zone its inductance varies with the current; consequently, the peak is more pronounced and the shape shows a cusp as shown in Fig. 11. It can be noted that the mean current is the same of the current imposed in linear operation to compare the behavior of the two inductors in the same operating conditions. The corresponding spectrum of the voltage noise evaluated on the measuring resistance of the LISN is shown in Fig. 12 with superimposed the different Class limits of the CISPR25 Standard. The RMS value of the noise current is 20.9 mA corresponding to a noise voltage on the 50Ω resistance of the LISN equal to 120.38 dBμV. The estimated voltage calculated by (9) with m=4 and α=2 is 96.30 dBμV; it is indicated by a dot on Fig. 12. Unlike the previous case study, the RMS value of the noise current at the frequency f_D =160 kHz practically coincides with the current spectrum line at 160 kHz and the odd harmonics (including the fundamental) are more relevant.

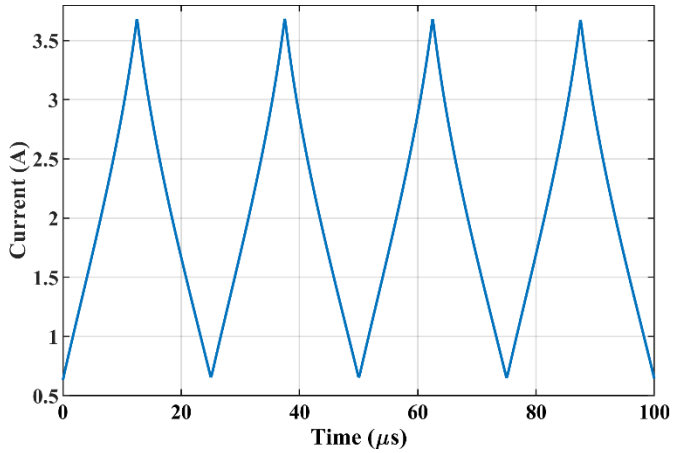

Fig. 11. Current flowing through the power inductor.

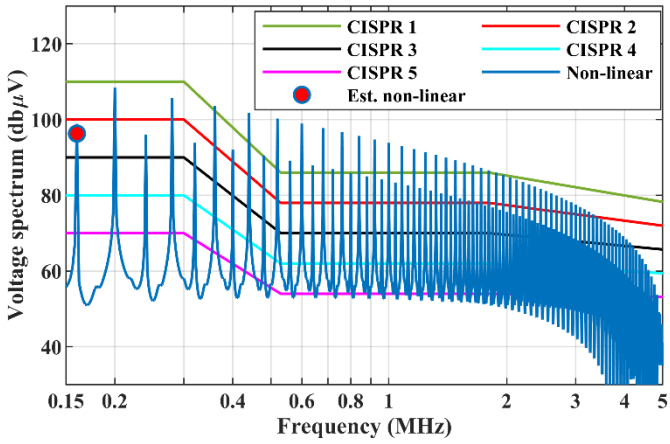

Fig. 12. Spectrum of the DM noise without filter

B. Filter design

The filter has been designed taking into account the required attenuation and the contribution of the odd harmonics considering both a single and a double stage and available commercial components. Also in this case, all the inductors have a rated current of 3 A and the capacitors have a polyester dielectric and a rated voltage of 50 V. Both inductors and capacitor belong to the same manufacturer: RSPRO and Nichicon respectively. The cost is referred to the purchase of a single component. The features of the components are summarized in Table II.

TABLE II. Components of the Filter for SMPS with Inductor in Non-Linear Operation

	Component	*Value*	*Size [mm³]*	*Cost [€]*	*Weight [g]*
Single stage	Inductor	150μH	5887	1.344	22.14
	Capacitor	820 nF	4388	2.182	6.02
Double stage	Inductor	47μH	2512	0.942	9.65
	Capacitor	100 nF	594	0.371	0.37

C. DM EMI with filter

The noise spectrum with the designed filters is shown in Fig. 13 where it can be appreciated that both filters achieve compliance, as expected.

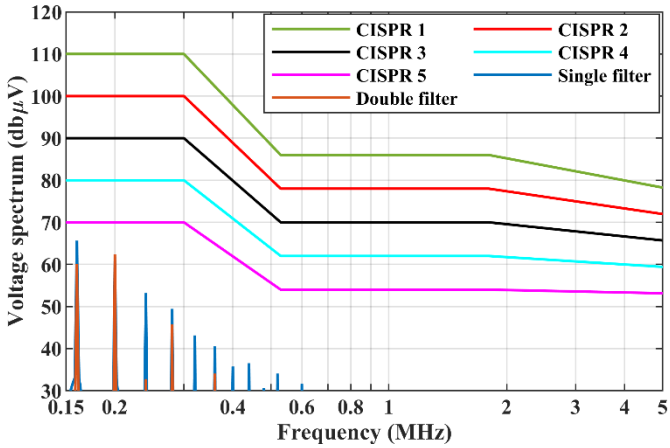

Fig. 13. Spectrum of the DM noise with filter

VIII. Comparison

The comparison of the power inductor and the filter is summarized in Table III. As for the single stage filter, it considers two inductors and one capacitor, whereas the double stage requires four inductors and two capacitors; the corresponding values are reported in Table I for the linear case and in Table II for the non-linear case, respectively.

It can be noted that, in any case, the non-linear operation of the inductor reduces the size and cost of the inductor but implies a higher cost of the filter. The double stage filter is preferable since it allows reducing cost and size. The overall comparison is shown in Table IV and in Fig. 14, where the best solutions are compared i.e., SMPS with linear inductor and single stage EMI filter and SMPS with non-linear inductor and double stage EMI filter. This last configuration requires an increase of 23% in size and of 23% in cost.

TABLE III. Comparison of the Components Considering Power Inductors and EMI Filter with Inductor in Linear and Non-Linear Operation

	SMPS operation	*Size [mm³]*	*Cost [€]*	*Weight [g]*
Power inductor	Linear operation	3240	3,56	5.72
	Non-linear operation	1620	2,67	3.44
EMI filter Single stage	Linear operation	7218	2.975	21.81
	Non-linear operation	16162	4.87	50.29
EMI filter Double stage	Linear operation	10256	4.32	38.67
	Non-linear operation	11236	4.51	39.34

TABLE IV. Overall Comparison of Size, Cost, and Weight

	Size [mm³]	*Cost [€]*	*Weight [g]*
SMPS with linear inductor and EMI filter (single stage)	10458	6.535	27.53
SMPS with non-linear inductor and EMI filter (double stage)	12856 (+23%)	8.07 (+23%)	42.78 (+55%)

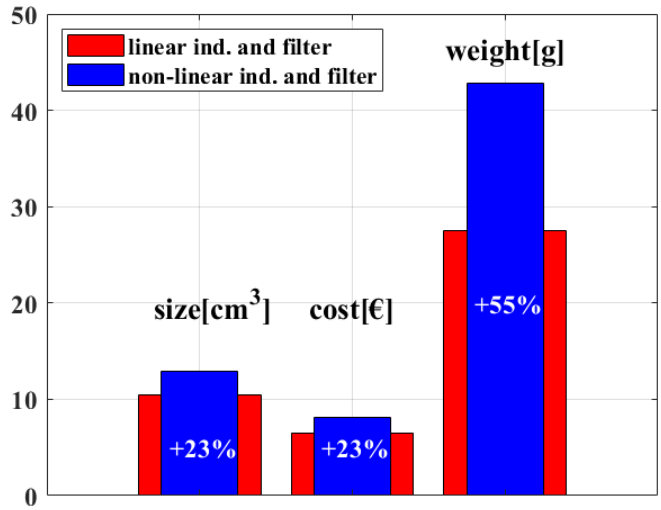

Fig. 14. Overall comparison of size, cost and weigth.

IX. Conclusions

In a SMPS, the exploitation of the power inductor in saturation allows reducing its size, cost and weight. On the other hand, it implies a re-design of the input EMI filter. In this case study, it has been shown that the compliance with class 5 CISPR 25 Standard requires an increase of the total cost, size and weight of the SMPS. Finally, these results demonstrate that the exploitation of the power inductor in saturation requires the verification of related parameters like weight, cost and size of the whole converter depending on the design requirements and the use of such inductors is not a guarantee of saving size, cost and weight.

References

[1] G. Di Capua and N. Femia, "A novel method to predict the real operation of ferrite inductors with moderate saturation in switching power supply applications," *IEEE Trans. Power Electron.*, vol. 31, no. 3, pp. 2456–2464, 2016, doi: 10.1109/TPEL.2015.2438952.

[2] L. Dai, W. Chen, R. Wang, Y. Yang, and Y. Zhou, "A New Approach for Improving Stability of Active CM EMI Filters for AC/DC Power Converters," Dec. 2018, doi: 10.1109/PEAC.2018.8590372.

[3] M. S. Perdigão, J. P. F. Trovão, J. M. Alonso, and E. S. Saraiva, "Large-Signal Characterization of Power Inductors in EV Bidirectional DC-DC Converters Focused on Core Size Optimization," *IEEE Trans. Ind. Electron.*, vol. 62, no. 5, pp. 3042–3051, 2015, doi: 10.1109/TIE.2015.2402632.

[4] F. Bizzarri, M. Lodi, A. Oliveri, A. Brambilla, and M. Storace, "A nonlinear inductance model able to reproduce thermal transient in SMPS simulations," in *Proceedings - IEEE International Symposium on Circuits and Systems*, May 2019, vol. 2019-May, pp. 1–5, doi: 10.1109/ISCAS.2019.8702418.

[5] K. Górecki and K. Detka, "Application of Average Electrothermal Models in the SPICE-Aided Analysis of Boost Converters," *IEEE Trans. Ind. Electron.*, vol. 66, no. 4, pp. 2746–2755, 2019, doi: 10.1109/TIE.2018.2847694.

[6] G. Vitale, G. Lullo, and D. Scire, "Thermal Stability of a DC/DC Converter With Inductor in Partial Saturation," *IEEE Trans. Ind. Electron.*, vol. 68, no. 9, pp. 7985–7995, Sep. 2021, doi: 10.1109/TIE.2020.3014580.

[7] D. Scire, G. Lullo, and G. Vitale, "Design and modeling of an interleaving boost converter with quasi-saturated inductors for electric vehicles," in *2020 AEIT International Conference of Electrical and Electronic Technologies for Automotive, AEIT AUTOMOTIVE 2020*, Nov. 2020, pp. 1–6, doi: 10.23919/aeitautomotive50086.2020.9307424.

[8] B. Narayanasamy and F. Luo, "A Survey of Active EMI Filters for Conducted EMI Noise Reduction in Power Electronic Converters," *IEEE Trans. Electromagn. Compat.*, vol. 61, no. 6, pp. 2040–2049, Dec. 2019, doi: 10.1109/TEMC.2019.2953055.

[9] J. W. T. Fan *et al.*, "Modeling and Experimental Assessment of the EMI Characteristics of Switching Converters with Power Semiconductor Filters," *IEEE Trans. Power Electron.*, vol. 35, no. 3, pp. 2519–2533, Mar. 2020, doi: 10.1109/TPEL.2019.2924551.

[10] M. Ferber, R. Mrad, F. Morel, G. Pillonnet, C. Vollaire, and A. Nagari, "Power Efficiency and EMI Attenuation Optimization in Filter Design," *IEEE Trans. Electromagn. Compat.*, vol. 60, no. 6, pp. 1811–1818, Dec. 2018, doi: 10.1109/TEMC.2017.2765921.

[11] Y. Liu *et al.*, "Evaluation on filter topologies in high power density converter design for power quality and EMI control," in *2015 Asia-Pacific International Symposium on Electromagnetic Compatibility, APEMC 2015*, Aug. 2015, pp. 20–23, doi: 10.1109/APEMC.2015.7175326.

[12] R. Wang, D. Boroyevich, H. F. Blanchette, and P. Mattavelli, "High power density EMI filter design with consideration of self-parasitic," in *Conference Proceedings - IEEE Applied Power Electronics Conference and Exposition - APEC*, 2012, pp. 2285–2289, doi: 10.1109/APEC.2012.6166141.

[13] G. Ala, G. C. Giaconia, G. Giglia, M. C. Di Piazza, and G. Vitale, "Design and Performance Evaluation of a High Power-Density EMI Filter for PWM Inverter-Fed Induction-Motor Drives," *IEEE Trans. Ind. Appl.*, vol. 52, no. 3, pp. 2397–2404, May 2016, doi: 10.1109/TIA.2016.2518129.

[14] R. W. Erickson and D. Maksimović, *Fundamentals of Power Electronics*. Boston, MA: Springer US, 2001.

[15] K. Raggl, T. Nussbaumer, and J. W. Kolar, "Guideline for a simplified differential-mode EMI filter design," *IEEE Trans. Ind. Electron.*, vol. 57, no. 3, pp. 1031–1040, Mar. 2010, doi: 10.1109/TIE.2009.2028293.

[16] D. Scirè, G. Lullo, and G. Vitale, "Non-Linear Inductor Contribution to Harmonic Spectrum in Power Converters," *Proc. XXVI Symp. Electromagn. Phenom. Nonlinear Circuits*, 2021.

[17] Coilcraft Inc., "SMT Power Inductors - DO5010H Series," 2020. https://www.coilcraft.com/en-us/products/power/unshielded-inductors/ferrite-drum-surface-mount/do/do5010h/ (accessed Sep. 01, 2020).

[18] Coilcraft Inc., "SMT Power Inductors - DO5040H Series," 2020. https://www.coilcraft.com/en-us/products/power/unshielded-inductors/ferrite-drum-surface-mount/do/do5040h/ (accessed Jan. 09, 2020).

[19] D. Scire, S. Rosato, G. Lullo, and G. Vitale, "A Temperature Dependent Non-Linear Inductor Model for a DC/DC Boost Converter," in *SMACD 2018 - 15th International Conference on Synthesis, Modeling, Analysis and Simulation Methods and Applications to Circuit Design*, Jul. 2018, no. September, pp. 237–240, doi: 10.1109/SMACD.2018.8434880.

[20] G. Lullo, D. Scirè, and G. Vitale, "Non-linear inductor modelling for a DC/DC buck converter," *Renew. Energy Power Qual. J.*, vol. 1, no. 15, pp. 686–693, 2017, doi: 10.24084/repqj15.433.

[21] G. Lullo, S. Rosato, D. Scirè, and G. Vitale, "Characterization of Non-linear Inductors Including Thermal Effects for Power Applications," *Renew. Energy Power Qual. J.*, vol. 1, no. April, pp. 728–734, Apr. 2018, doi: 10.24084/repqj16.446.

[22] International Electrotechnical Commission (IEC), "CISPR 25:2016-Vehicles, boats and internal combustion engines – Radio disturbance characteristics – Limits and methods of measurement for the protection of on-board receivers," CISPR 25:2016, 2016.

[23] M. C. D. Piazza, A. Ragusa, and G. Vitale, "Common mode EMI propagation in high voltage DC supplied induction motor drives for electric vehicles application," in *2009 IEEE International Electric Machines and Drives Conference, IEMDC '09*, 2009, pp. 647–652, doi: 10.1109/IEMDC.2009.5075274.

[24] M. Ventimiglia, D. Scirè, G. Lullo, and G. Vitale, "A Measurement System for Power Inductors in Non-Linear Operating Conditions," in *IEEE 30th International Symposium on Industrial Electronics (ISIE)*, 2021, pp. 1–6.

[25] D. Scirè, G. Vitale, M. Ventimiglia, and G. Lullo, "Non-Linear Inductors Characterization in Real Operating Conditions for Power Density Optimization in SMPS," *Energies*, vol. 14, no. 13, 2021, doi: 10.3390/en14133924.

[26] G. Giglia *et al.*, "Automatic EMI filter design for power electronic converters oriented to high power density," *Electron.*, vol. 7, no. 1, 2018, doi: 10.3390/electronics7010009.

[27] Y. Maillet, R. Lai, S. Wang, F. Wang, R. Burgos, and D. Boroyevich, "High-density EMI filter design for dc-fed motor drives," *IEEE Trans. Power Electron.*, vol. 25, no. 5, pp. 1163–1172, 2010, doi: 10.1109/TPEL.2009.2039004.

[28] R. Lee Ozenbaugh and T. M. Pullen, *EMI filter design: Third edition*. CRC Press, 2017.